Experimental study of temperature fluctuations in forced stably stratified turbulent flows

Igal Gluzman
Supervisors: Prof. Tov Elperin & Prof. Alexander Eidelman

Laboratory of Turbulent Multiphase Flows
Department of Mechanical Engineering
Ben-Gurion University of the Negev

igal.gluzman@gmail.com

August 6, 2013

Overview

A fog-ridden, pooled shallow SBL in a mountain valley (SBL- stable boundary layer)

Figure 1.1 : WHITHER THE STABLE BOUNDARY LAYER,"A Shift in the Research Agenda", by H. J. S. Fernando and J. C. Weil.

Stratified flows

Equation of motion of the fluid element:

$$\frac{d^2\delta z}{dt^2} + \frac{g}{\Theta_{P,s}}\frac{d\Theta_{P,s}}{dz}\delta z = 0. \tag{1}$$

Solution:

$$\delta z = \delta z_0 e^{\sqrt{-N^2}t} = \delta z_0 e^{iNt} = \delta z_0 \left[\cos\left(Nt\right) + i\sin\left(Nt\right)\right] \ . \tag{2}$$

Brunt Väisälä frequency

$$N^2 = \frac{g}{\Theta_{P,s}}\frac{d\Theta_{P,s}}{dz} > 0. \tag{3}$$

Stratified flows

The potential temperature Θ_P is defined to be the temperature a parcel of fluid at local temperature, T and pressure, p, would have if it were expanded or compressed adiabatically to a standard pressure p_0, i.e.

$$\Theta_P = T\left(\frac{p_0}{p}\right)^{(\gamma-1)/\gamma}, \tag{4}$$

$$\frac{d\Theta_P}{dz} = \frac{\Theta_P}{T}\left(\frac{dT}{dz} + \frac{g}{C_p}\right). \tag{5}$$

The quantity $\gamma_a = \frac{g}{C_p}$ is called the dry adiabatic gradient of temperature, that for the Earth's atmosphere, assumes the value $0.01\,K/m$. Hence we can estimate $dT/dz \gg g/C_p$:

$$\frac{1}{\Theta_P}\frac{d\Theta_P}{dz} \approx \frac{1}{T}\frac{dT}{dz}. \tag{6}$$

Stratified flows

Gradient Richardson number:

$$Ri = \frac{N^2}{S^2}\,, \tag{7}$$

S is the total mean velocity vertical shear $S^2 = \left(\frac{\partial U_z}{\partial z}\right)^2 + \left(\frac{\partial U_x}{\partial z}\right)^2$.

Turbulent Richardson number

$$Ri_T = \left(\frac{\tau_z}{\tau_b}\right)^2 = N^2\tau_z^2\,, \tag{8}$$

Vertical turbulent time $\tau_z = \ell_z/u_{rms,z}$; Buoyancy time scale $\tau_b = 1/N$.

Boussinesq approximation

Under the assumption $\delta\rho/\rho_s \ll 1$, the Boussinesq approximation holds. approximation introduced by Boussinesq (1903) is based on the following assumptions:

(i) Neglecting variations of density in so far as they affect inertia but retaining them in the buoyancy terms. Hence the density in the inertial term is taken to be equal to the reference state variable.

(ii) variations of fluid properties are also neglected in this approximation such as dynamic viscosity μ.

(iii) Vertical size of the flow domain is much less than any scale height L_ξ, which can be defined as $L_\xi = \xi[d\xi/dz]^{-1}$, where ξ represents any one of the state variables: density (ρ), temperature (T), or pressure (p).

(iv) Fluctuating density changes due to local pressure variations must also be negligible. This assumption implies that the fluid can be treated as incompressible, and therefore excludes sound and shock waves.

Reynolds Averaged Navier-Stokes (RANS) approach

System of equations for the mean flow variables:
(+Boussinesq approximation)

$$\frac{\partial U_i}{\partial x_i} = 0\,, \tag{9}$$

$$\frac{\partial U_i}{\partial t} + U_j \frac{\partial U_i}{\partial x_j} = -\frac{1}{\bar{\rho}} \frac{\partial P}{\partial x_i} + \frac{\partial}{\partial x_j} \left[2\nu S_{ij} - \langle u_i u_j \rangle \right] + \frac{\delta \bar{\rho}}{\bar{\rho}} g_i\,, \tag{10}$$

$$\frac{\partial T}{\partial t} + U_j \frac{\partial T}{\partial x_j} + \frac{\partial \langle u_j \theta \rangle}{\partial x_j} = -\frac{1}{\bar{\rho} C_p} \frac{dP}{dt} + \alpha \frac{\partial^2 T}{\partial x_i^2} + \frac{2\mu}{\bar{\rho} C_p} \left(S_{ij} S_{ij} + \langle s_{ij} s_{ij} \rangle \right)\,, \tag{11}$$

where $S_{ij} = \frac{1}{2}\left(\frac{\partial U_i}{\partial x_j} + \frac{\partial U_j}{\partial x_i} \right)$; $\quad s_{ij} = \frac{1}{2}\left(\frac{\partial u_i}{\partial x_j} + \frac{\partial u_j}{\partial x_i} \right)$.

The closure problem

Reynolds stresses $\langle u_i u_j \rangle$ and turbulent heat flux $\langle u_i \theta \rangle$.

Energy- and flux-budget (EFB) turbulence closure model

In our theoretical analysis we use three budget equation for the turbulent kinetic energy $E_K = \langle {u_i}^2 \rangle / 2$, for the turbulent heat flux $F_i = \langle u_i \theta \rangle$ and for the temperature fluctuations $E_\theta = \langle \theta^2 \rangle / 2$:

$$\frac{DE_K}{Dt} + \nabla_j \Phi_j^{(K)} = -\langle u_i u_j \rangle \nabla_j U_i + \mathrm{P}_{G,K} + \frac{1}{2} Q_{ii} + \beta F_z - \varepsilon_K, \qquad (12)$$

$$\frac{DF_i}{Dt} + \nabla_j \Phi_{ij}^{(F)} = \beta_i \langle \theta^2 \rangle - \frac{1}{\rho} \langle \theta \nabla_i p' \rangle - \langle u_i u_j \rangle \nabla_i \overline{T} - (F_j \cdot \nabla_j) U_i - \varepsilon_i^{(F)}, \qquad (13)$$

$$\frac{DE_\theta}{Dt} + \nabla_j \Phi_j^{(\theta)} = -(F_j \cdot \nabla_j) \overline{T} - \varepsilon_\theta. \qquad (14)$$

Energy- and flux-budget (EFB) turbulence closure model

The terms $\Phi_j^{(K)}$, $\Phi_{ij}^{(F)}$ and $\Phi_j^{(\theta)}$ include the third-order moments.
Dissipation terms ε_K, $\varepsilon_i^{(F)}$, ε_θ. Following Kolmogorov (1941):

$$\varepsilon_K = \frac{E_K}{C_K \tau_0}, \ \varepsilon_i^{(F)} = \frac{F_i}{C_F \tau_0}, \ \varepsilon_\theta = \frac{E_\theta}{C_P \tau_0}, \tag{15}$$

C_K and C_P are dimensionless constants of the order of 1.

We estimate the terms $\beta_i \langle \theta^2 \rangle - \rho^{-1} \langle \theta \nabla_i p' \rangle$, in Eq. (13) as:

$$\beta_i \langle \theta^2 \rangle - \rho^{-1} \langle \theta \nabla_i p' \rangle \approx C_\theta \beta_i \langle \theta^2 \rangle . \tag{16}$$

Energy- and flux-budget (EFB) turbulence closure model

Turbulent potential energy (TPE), $E_P = (\beta^2/N^2)\, E_\theta$:

$$\frac{DE_p}{Dt} + \nabla_j \Phi_j^{(P)} = \mathrm{P}_P - \beta F_z - \varepsilon_p, \tag{17}$$

where, $\beta = g/T$.

Turbulent total energy (TTE), $E = E_K + E_P$:

$$\frac{DE}{Dt} + \nabla_j \Phi_j \quad = \quad \mathrm{P}_P - \langle u_i\, u_j \rangle \nabla_j U_i + \mathrm{P}_{G,K} - \varepsilon. \tag{18}$$

The concept of the total turbulent energy is very useful in analysis of stratified turbulent flows.

Energy- and flux-budget (EFB) turbulence closure model

Energy- and flux-budget (EFB) turbulence closure model reveals three flow regimes:

1. Weakly stable regime, where $Ri \ll 1$, with strong turbulence.
2. Very stable regime, when $Ri > 1$, with weak turbulence, capable of transporting momentum but much less efficient in transporting heat.
3. Transition regime, $0.1 < Ri < 1$, which separates two regimes of essentially different nature but both turbulent.

EFB local model predictions for our experiments

Applying EFB model in our study can be simplified under the following assumption:

1. Steady-state, homogeneous regime. In equilibrium turbulence regime we can neglect the third-order transport terms, so that the l.h.s. in all budget equations become zero.
2. The diagonal components of the tensor $\langle u_i u_j \rangle$ are much larger than the off-diagonal components: $\langle u_i u_i \rangle \gg \langle u_i u_j \rangle_{i \neq j}$.
3. We assume that turbulent times are approximately equal, i.e. $\tau_x \approx \tau_y \approx \tau_z = \tau_0$.

EFB local model predictions for our experiments

Eq. (13) yields the components of the turbulent heat flux:

$$F_x = -D_x^T \ \nabla_x \overline{T},\ F_y = -D_y^T \nabla_y \overline{T},\ \ F_z = -D_z^T \nabla_z \overline{T} + C_\theta\, C_F\, \tau_0\, \beta\, \langle \theta^2 \rangle, \quad (19)$$

where $D_x^T = C_F\, \tau_0\, \langle u_x^2 \rangle, \quad D_y^T = C_F\, \tau_0\, \langle u_y^2 \rangle, \quad D_z^T = C_F\, \tau_0\, \langle u_z^2 \rangle.$

Eq. (14) yields:

$$\langle \theta^2 \rangle = -2\, \tau_0\, (F_j \cdot \nabla_j) \overline{T}, \quad (20)$$

Substituting the components of F_i (Eq. (19)) into Eq. (20), we obtain:

$$\frac{\ell_* \nabla_* T}{\sqrt{\langle \theta^2 \rangle}} = \frac{1}{\sqrt{2 C_F}} = \text{const}, \quad (21)$$

where

$$[\ell_* \nabla_* T]^2 \equiv [(\ell_x \nabla_x \bar{T})^2 + (\ell_y \nabla_y \bar{T})^2 + (\ell_z \nabla_z \bar{T})^2] \times [1 + 2 C_\theta C_F Ri_T]^{-1}. \quad (22)$$

EFB local model predictions for our experiments

The budget equation for the vertical turbulent kinetic energy $E_z = \langle u_z^2 \rangle / 2$

$$\frac{DE_z}{Dt} + \nabla_j \Phi_j^{(z)} = \mathrm{P}_{G,z} + \beta F_z + \frac{1}{2} Q_{zz} - \varepsilon_z, \tag{23}$$

we arrive at the following equation

R.m.s of vertical turbulent velocity

$$\sqrt{\langle u_z^2 \rangle} = \sqrt{\left\langle u_{z,iso}^2 \right\rangle - C_u \beta \ell_z \sqrt{\langle \theta^2 \rangle}}, \tag{24}$$

where, C_u is an empirical constant.

Experimental setup

- Chamber dimensions: $26 \times 58 \times 26$ cm^3.
- Air flow ($\mathrm{Pr} = 0.71$).
- Grids: amplitude of 6.1 cm (grid stroke); random phase.
- Aluminium heat exchangers: cooled bottom wall; heated top wall.

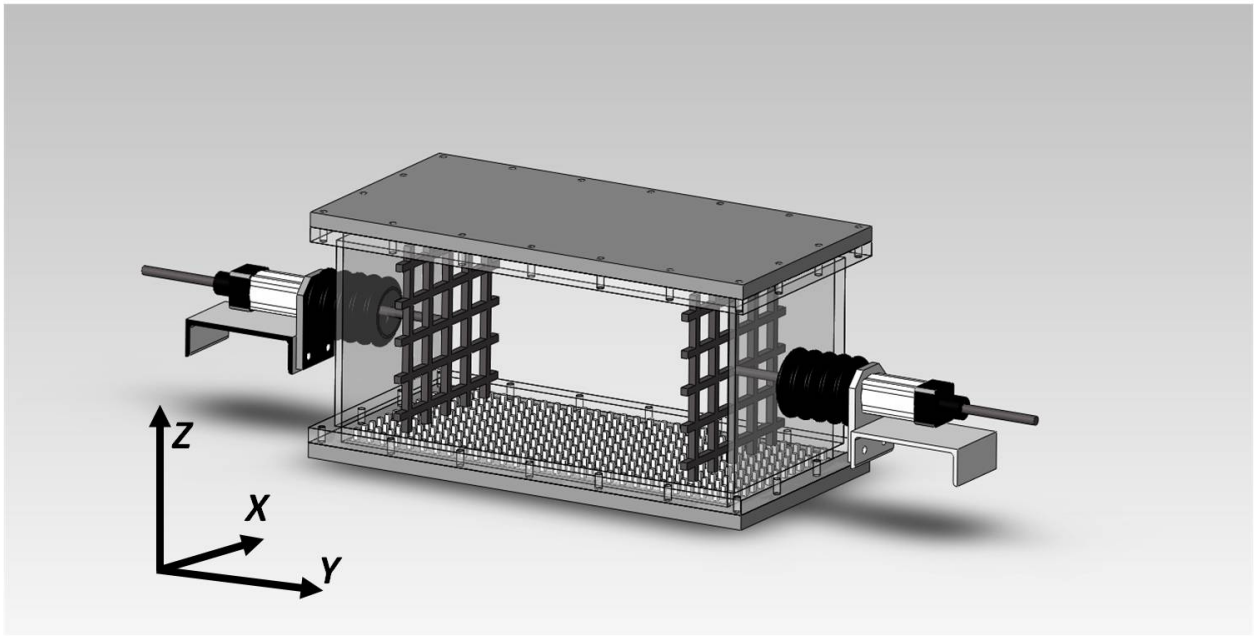

Figure 2.1 : Rectangular chamber with two oscillating grids.

Experimental setup

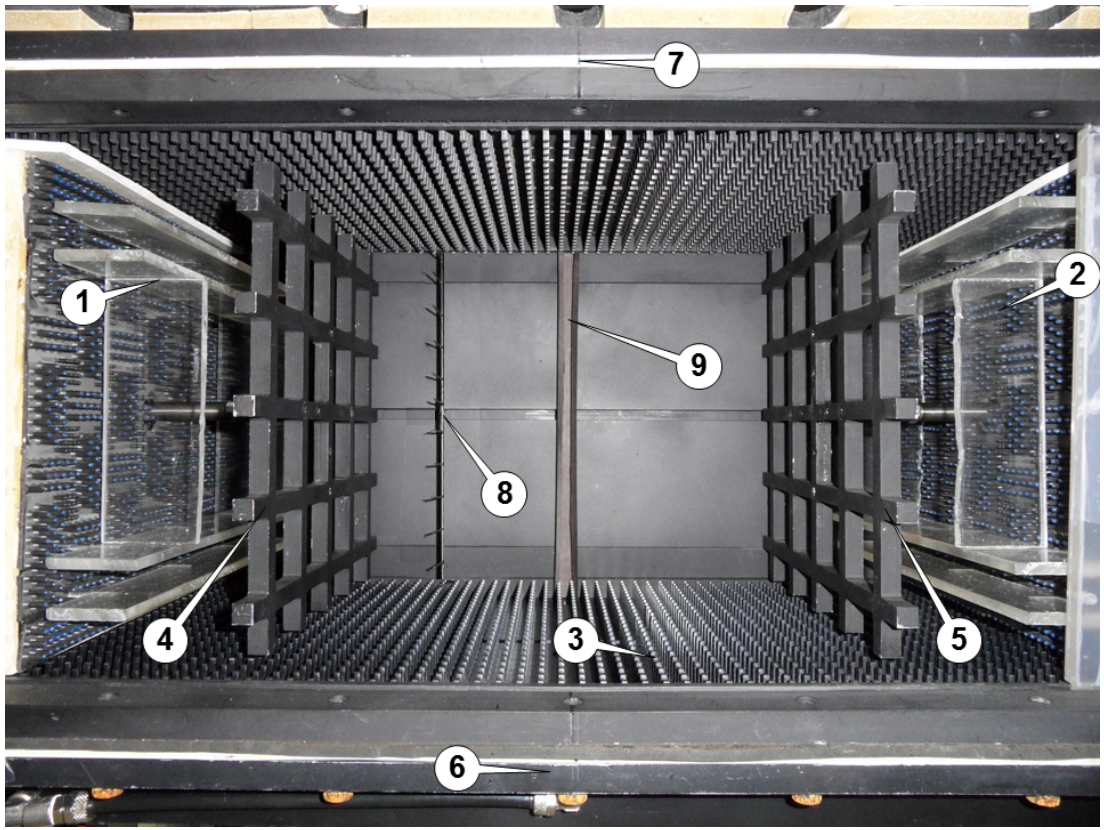

Figure 2.2 : Photo of the test section with temperature measuring probe. 1,2- vertical partitions, 3- rectangular fins, 4,5- oscillating grids, 7- heated top wall, 8- temperature measuring probe, 9- light trap.

Temperature measuring in the experiments

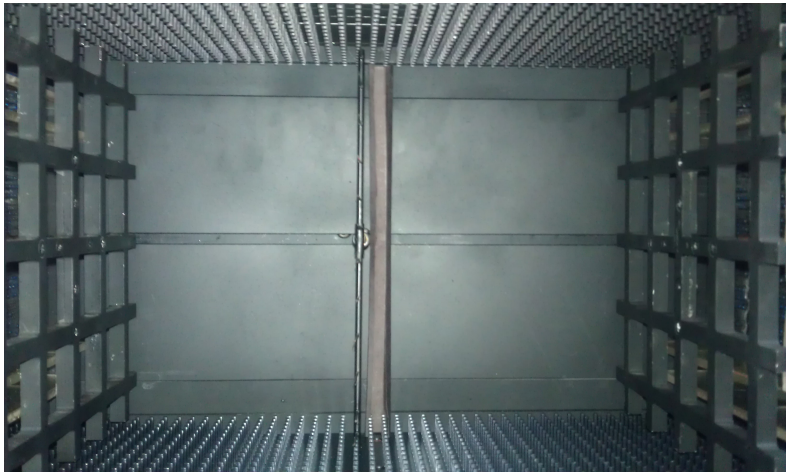

Figure 2.3 : Central vertical rod position of temperature measuring device.

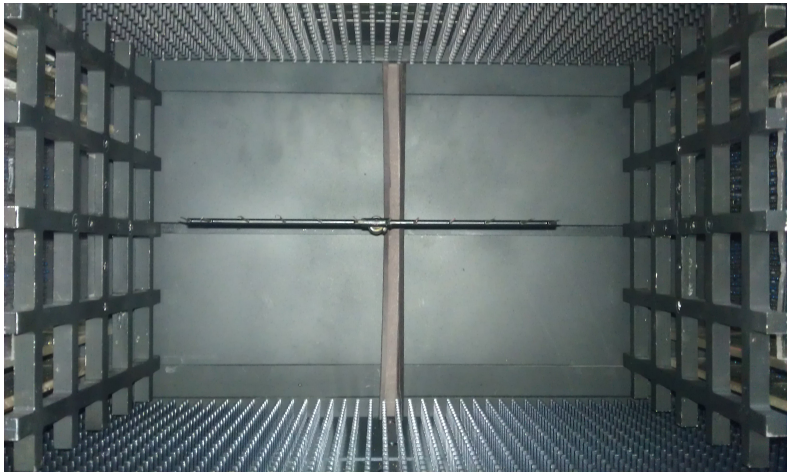

Figure 2.4 : Central horizontal rod position of temperature measuring device.

Grid oscillations frequencies:

$$f = 1, 2.5, 4.5, 6.5, 8.5, 10.5\, Hz\,,$$

Temperature differences:

$$\Delta T = 12, 20, 30, 40, 50\, K\,.$$

Temperature measuring in the experiments

- Exposed junction type thermocouples (fastest response time).
- Heat-exchanger:
  - 4 K-type (Chromel - Alumel) thermocouples.
  - Sensitivity of $\approx 39\ \mu V/K$.
- Air flow:
  - 12 E-type (Chromel - Constantan) thermocouples.
  - Sensitivity of $\approx 75\ \mu V/K$.
  - Diameter of 0.125 mm.
  - Response time of ≈ 0.08 sec (integral time scale: $\tau \approx 0.2 \div 1$ sec).
- Hardware: Agilent 34970A data logger; Software: LabView 7.0.
- A sequence of 500 temperature readings with time difference of $\Delta t = 0.8$ sec.
- Accuracy: 0.07% for absolute temperature measurements; Measuring system noise r.m.s equals $0.04\,^{\circ}C$.

Velocity fields measurements in the experiments

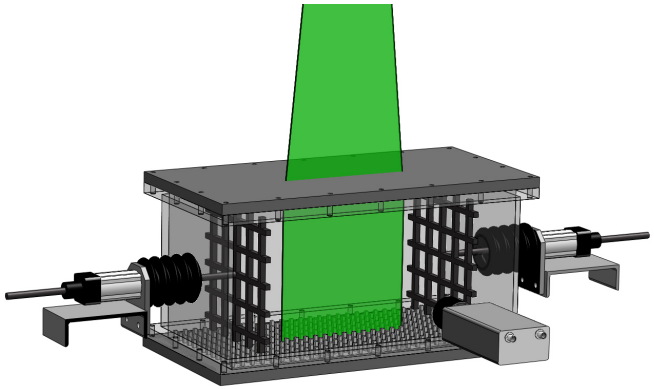

Figure 2.5 : Front view set-up: yz plane illumination at the center of the cavity.

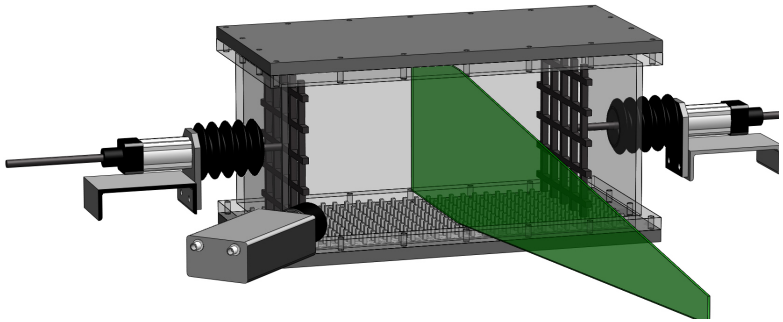

Figure 2.6 : Side view set-up: xz plane illumination at the center of the cavity.

Grid oscillations frequencies:

$$f = 1, 2.5, 4.5, 6.5, 8.5, 10.5\, Hz\,,$$

Temperature differences:

$$\Delta T = 0, 50\, K\,.$$

Velocity fields measurements in the experiments

$$u_{rms,x} \equiv \sqrt{\langle u_x^2 \rangle} = \left(\frac{\tan^2(\beta)}{b^2} + 1 \right)^{-1/2} \sqrt{\left\langle \left(u_{x,c}^* \right)^2 \right\rangle}.$$

$b(f) = u_{rms,z}(f)/u_{rms,y}(f)$. (front view)
It assumed that $u_{rms,z} \simeq u_{rms,x}$ in isothermal case.

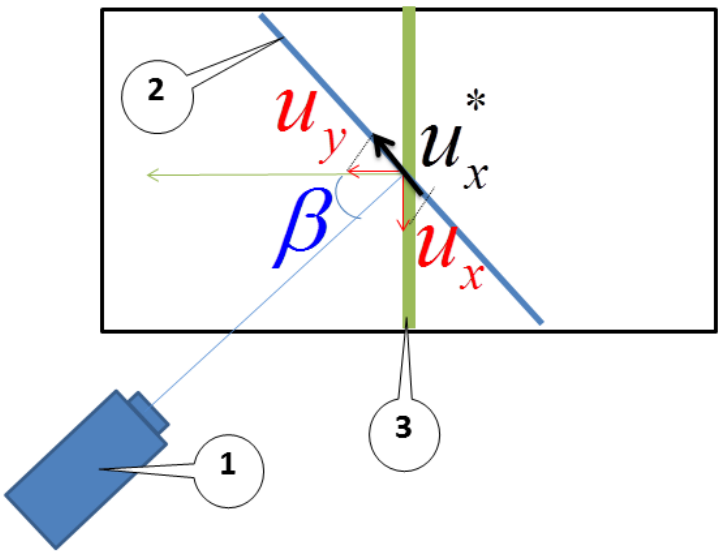

Figure 2.7 : Schematic view on xz plane illumination from above. 1-CCD camera, 2-camera optical axis, 3-light sheet in test section.

Particle image velocimetry techniques

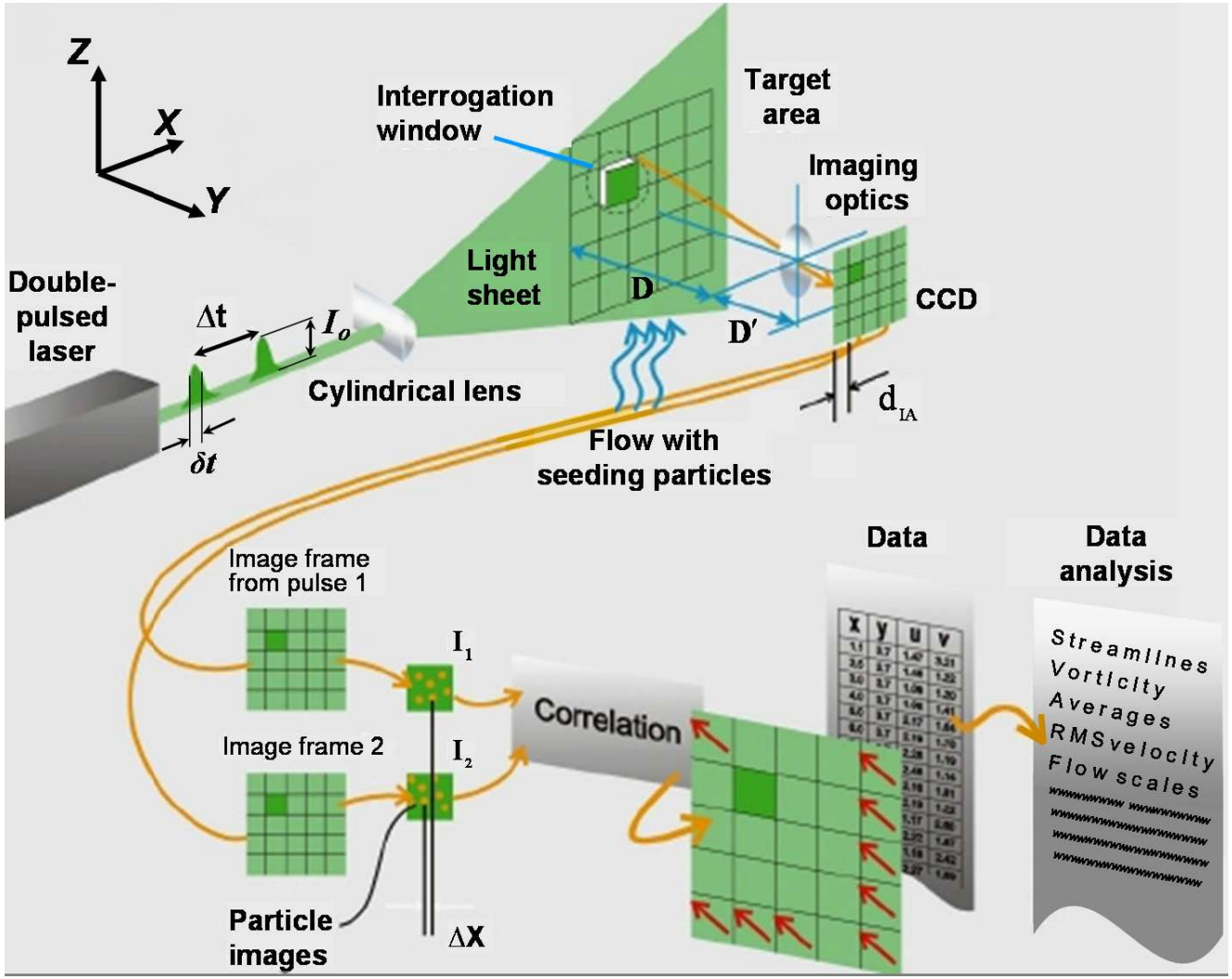

Figure 2.8 : Particle Image Velocimetry technique.

Velocity fields measurements in the experiments

- Software package LaVision DaVis 7.
- Nd-YAG laser (Continuum Surelite 2×170 mJ).
- A dual-frame-technique for cross-correlation processing:

$$\Phi_C(m,n) = \sum_{i=0}^{M-1} \sum_{j=0}^{N-1} g_1(i,j)\, g_2(i+m, j+n).$$

- Tracer: incense smoke ($\rho_p/\rho \sim 10^3$, mean diameter $\approx 0.7\mu$m).
- LaVision Flow Master III system: 12 bit digital CCD cameras:
  - xz plane: pixel size $6.7\,\mu$m $\times 6.7\,\mu$m; frame size 1280×1024 pixels.
  - yz plane: pixel size $6.45\,\mu$m $\times 6.45\,\mu$m; frame size 1376×1040 pixels.
- Spatial resolution:
  xz plane: $a = 0.2269\,mm/pixel$; yz plane: $a = 0.2064\,mm/pixel$.

Velocity fields measurements in the experiments

- Average tracer displacement:
  xz plane: 0.44 pixel; yz plane: 1.12 pixel.
- Analyzed with 32×32 interrogation windows with size of 32×32 pixels.
- Accuracy of the correlation peak detection in the interrogation window: 1/10 pixel.
- The accuracy of r.m.s velocity measurements:
  xz plane 6.1%; yz plane:2.1%.
- Series of images:
  xz-plane: 150 pairs; yz-plane: 520 pairs.
- Time interval between pairs of images: $\Delta t = 1$ sec.
- velocity maps considered as independent ($\Delta t > \tau = 0.2 \div 1$ sec).

Results of PIV measurements

Spatial distribution of rms velocity components in the central part of the probed region are quite homogeneous and nearly quite isotropic.

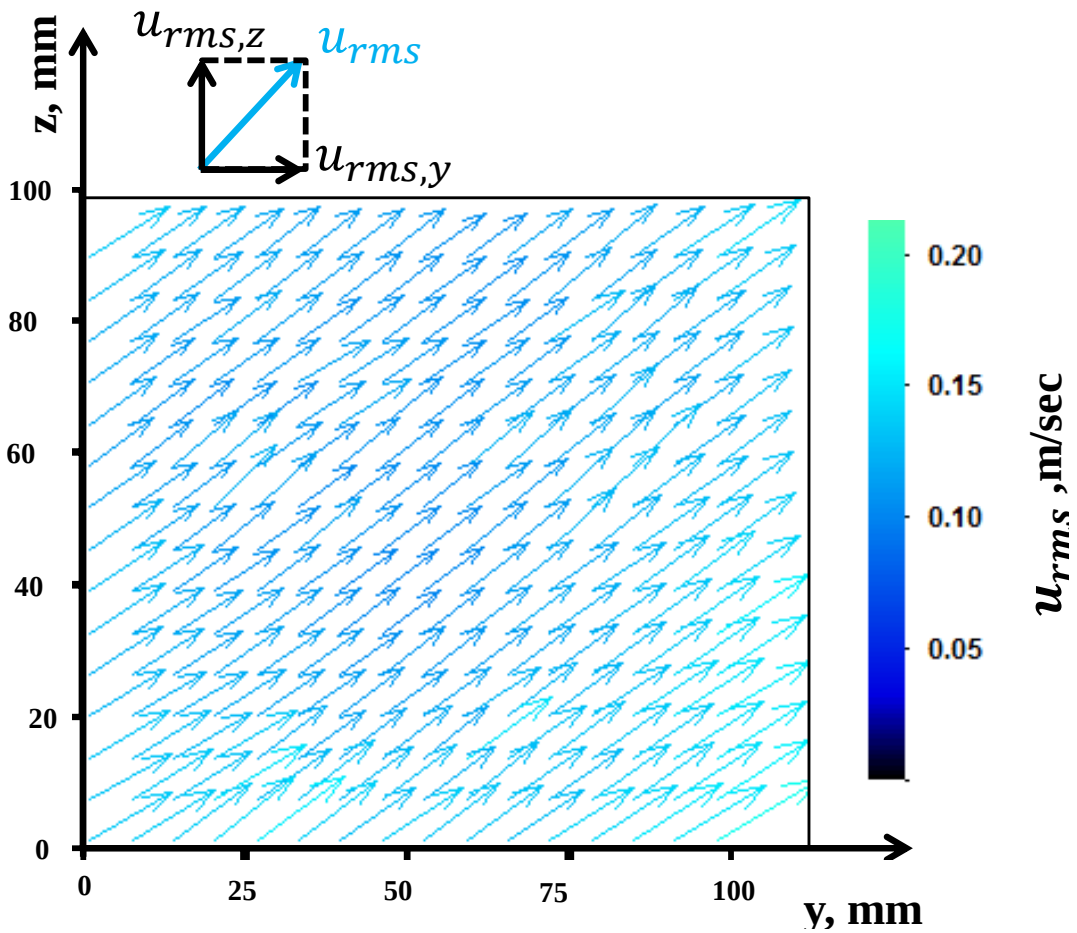

Figure 3.1 : R.m.s velocity map in central region ($f = 10.5\,\text{Hz}, \triangle T = 50$ K) in yz plane.

Results of PIV measurements

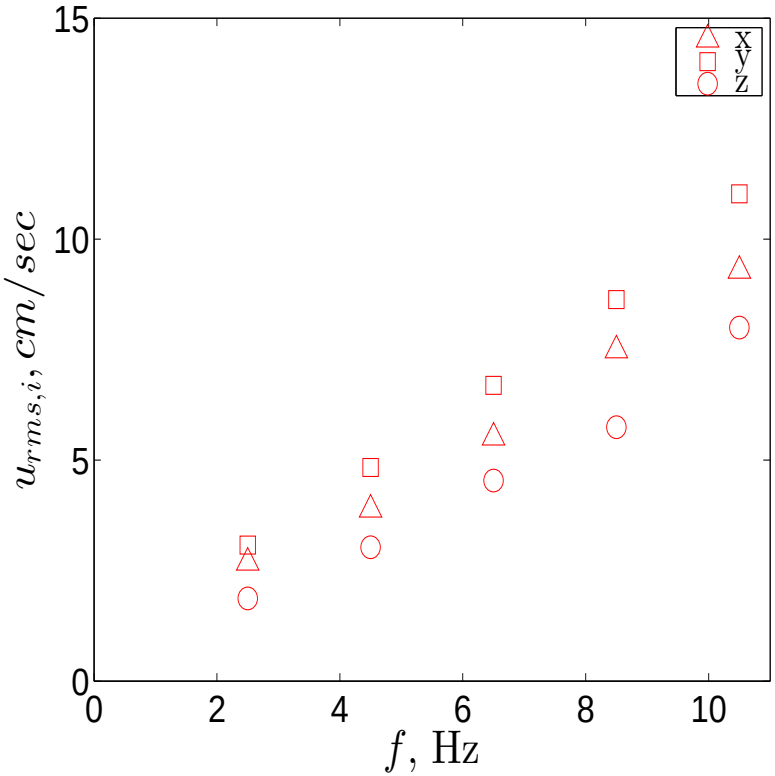

Figure 3.2 : R.m.s velocity components ($\triangle T = 50$ K): $u_{\mathrm{rms,x}} = \sqrt{\langle u_x^2 \rangle}$, $u_{\mathrm{rms,y}} = \sqrt{\langle u_y^2 \rangle}$, $u_{\mathrm{rms,z}} = \sqrt{\langle u_z^2 \rangle}$.

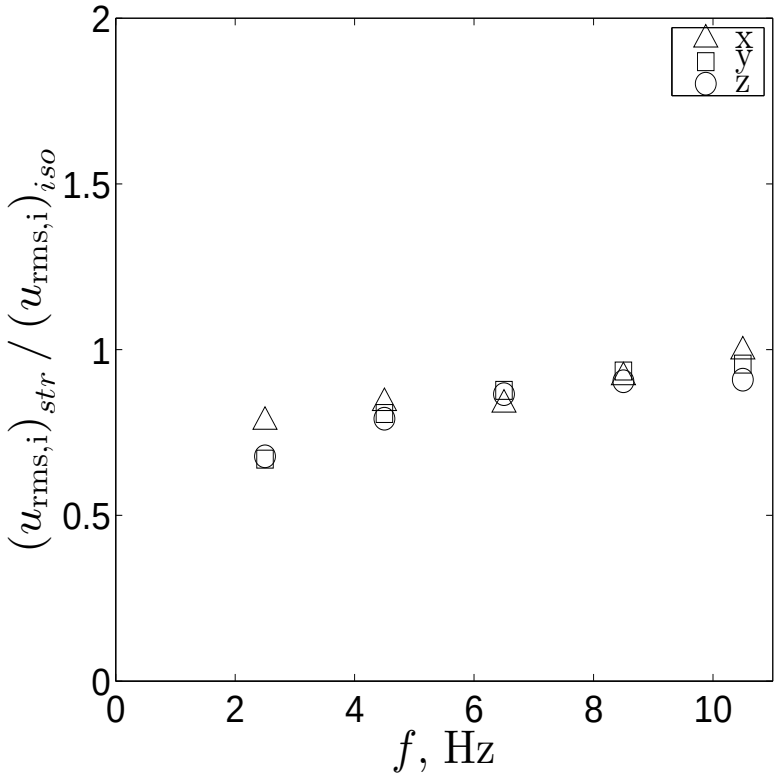

Figure 3.3 : Normalized r.m.s velocity $\left(u_{\mathrm{rms,i}}\right)_{str} / \left(u_{\mathrm{rms,i}}\right)_{iso}$.

Results of PIV measurements

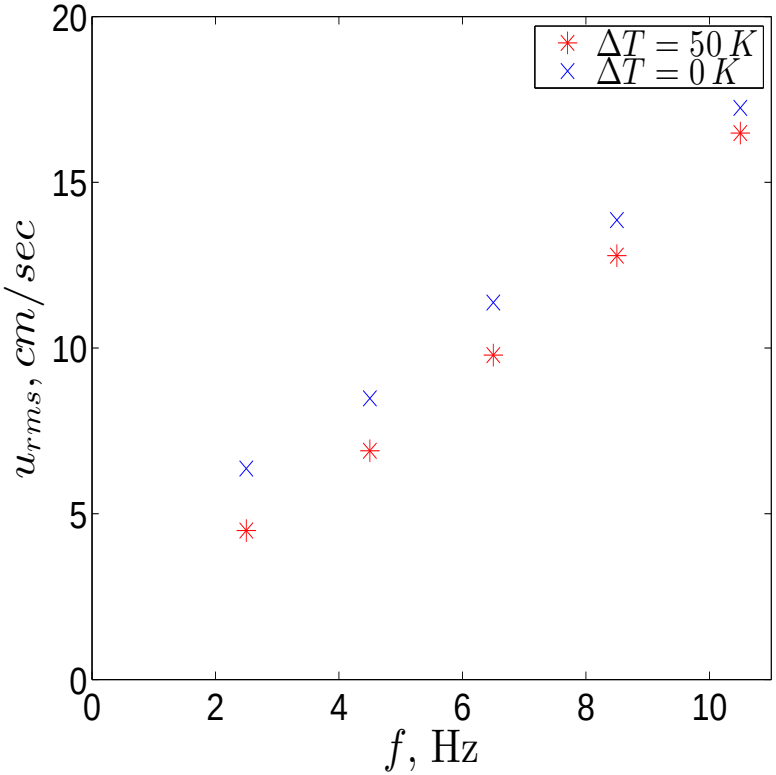

Figure 3.4 : R.m.s. turbulent velocity:
$u_{\mathrm{rms}} = \left[\langle u_x^2 + u_y^2 + u_z^2 \rangle\right]^{1/2}$.

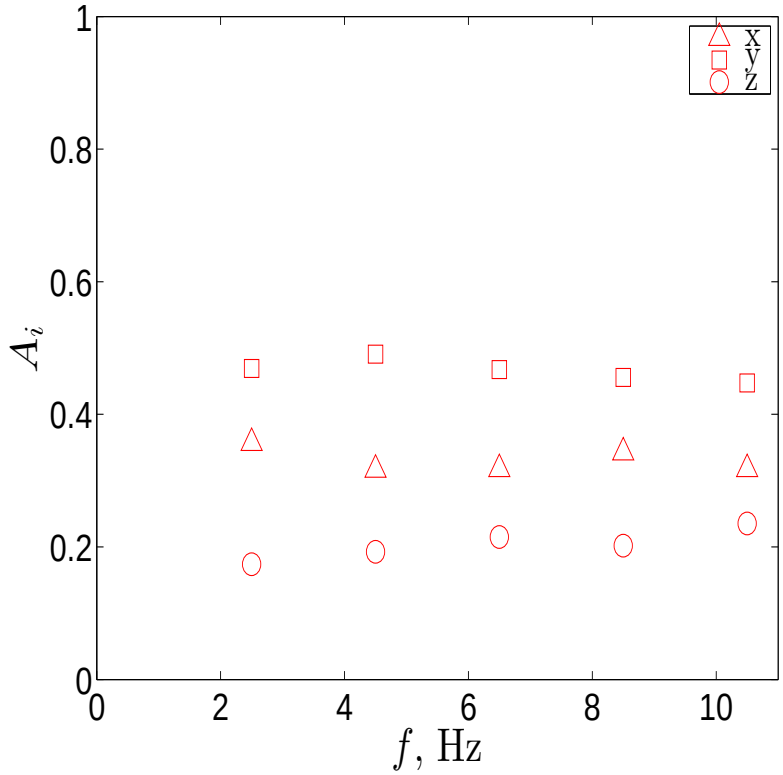

Figure 3.5 : Anisotropy ($\triangle T = 50\,\mathrm{K}$): $A_x = \langle u^2_{\mathrm{rms,x}} \rangle / u^2_{\mathrm{rms}}$, $A_y = \langle u^2_{\mathrm{rms,y}} \rangle / u^2_{\mathrm{rms}}$, $A_z = \langle u^2_{\mathrm{rms,z}} \rangle / u^2_{\mathrm{rms}}$.

Results of PIV measurements

$$R_{yy}(x_0, y, z_0) = \langle u_y(x_0, y_0, z_0)\, u_y(x_0, y_0 + \vec{y}, z_0)\rangle / \langle u_y^2(x_0, y_0, z_0)\rangle.$$

R_{yy} in yz plane: $R_{yy} = \frac{1}{z_2 - z_1} \int_{z_1}^{z_2} R_{yy}(z)\, dz.$

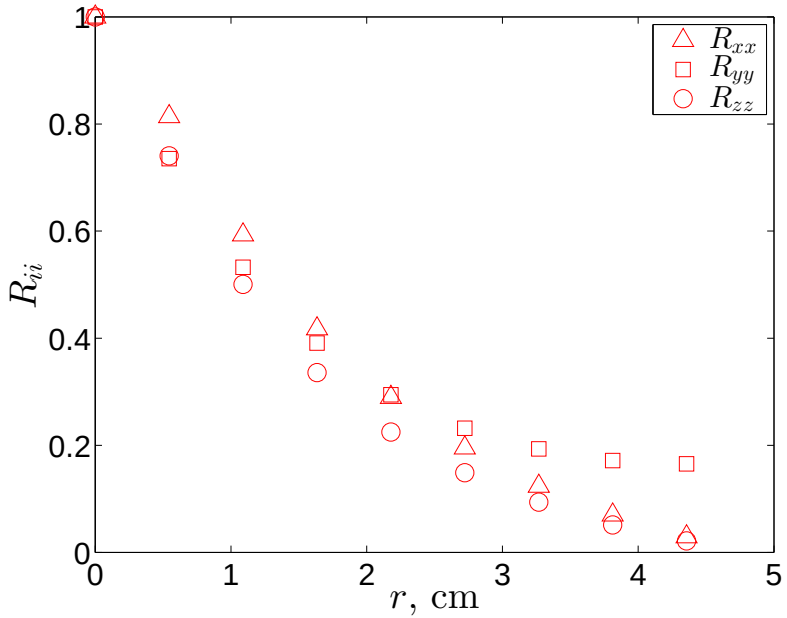

Figure 3.6 : R_{yy} and R_{zz} in yz plane and R_{xx} in xz plane ($\triangle T = 50\,\mathrm{K}$, $f = 10.5\,\mathrm{Hz}$).

Results of PIV measurements

$$\ell_i = \int_0^\infty R_{ii}(r)\,dr \approx \int_0^\infty e^{-\alpha r}\,dr = \frac{1}{\alpha}.$$

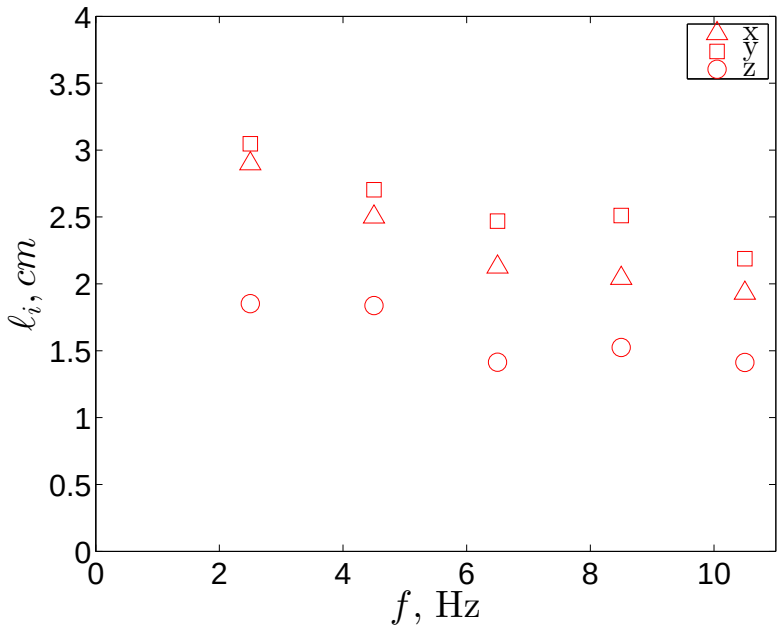

Figure 3.7 : Integral scales of turbulence ℓ_i ($\triangle T = 50$ K).

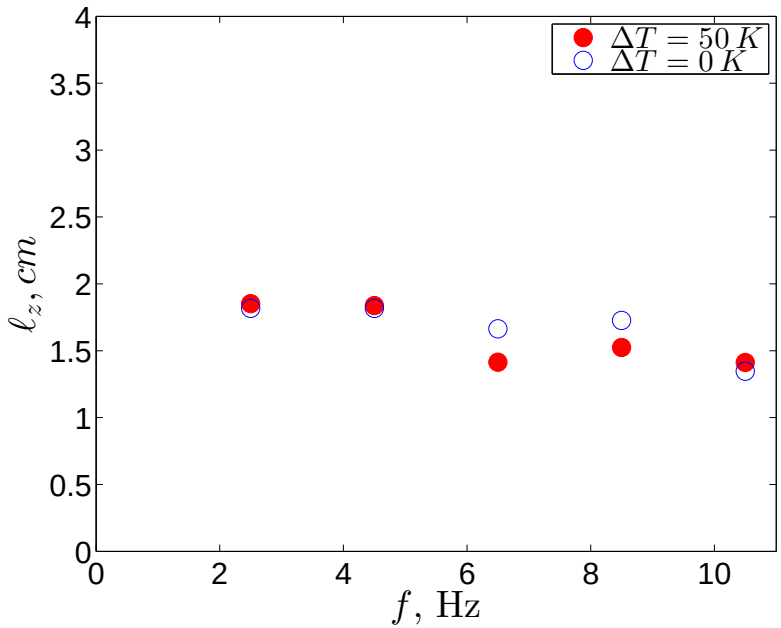

Figure 3.8 : Vertical integral scale of turbulence ℓ_z.

Results of PIV measurements

$Re = \ell\, u_{rms}/\nu_{air}$, where $\ell = (\ell_x^2 + \ell_y^2 + \ell_z^2)^{1/2}$ and $\nu_{air} \approx 0.15\, cm^2/s$.

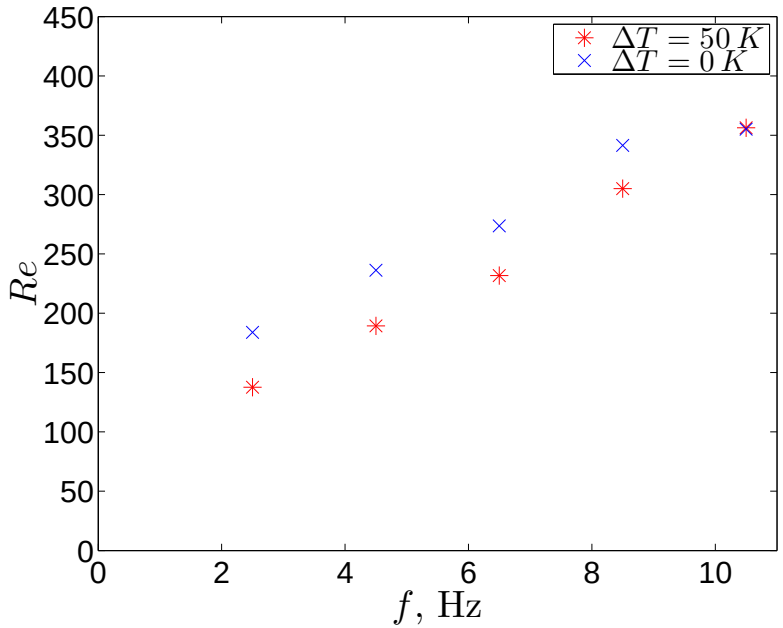

Figure 3.9 : Turbulent Reynolds number $Re = \ell\, u_{rms}/\nu_{air}$.

Results of PIV measurements

The turnover time (turbulent time τ_i) was estimated as $\ell_i/u_{rms,i}$

$\varepsilon_x = A\langle u_x^2\rangle^{3/2}/\ell_x$, $\varepsilon_y = A\langle u_y^2\rangle^{3/2}/\ell_y$, and $\varepsilon_z = A\langle u_z^2\rangle^{3/2}/\ell_z$, where $A \approx 1$

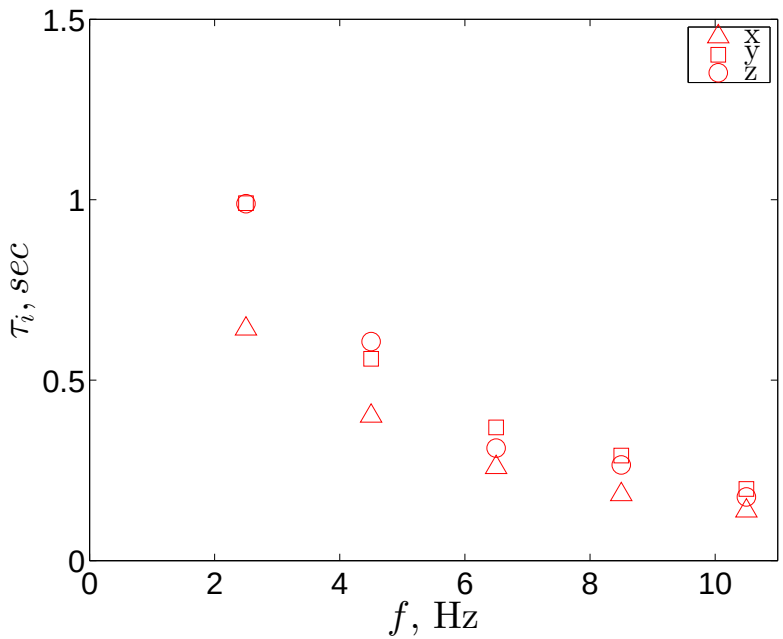

Figure 3.10 : Turbulent times $\tau_i = \ell_i/u_{rms,i}$ ($\triangle T = 50$ K).

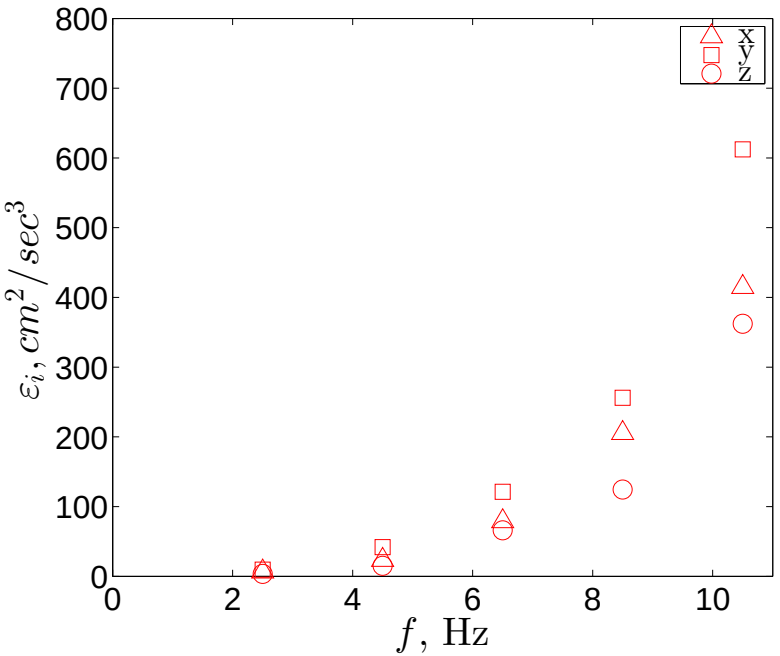

Figure 3.11 : Dissipation rates of turbulent kinetic energies ε_i ($\triangle T = 50$ K).

Results of PIV measurements

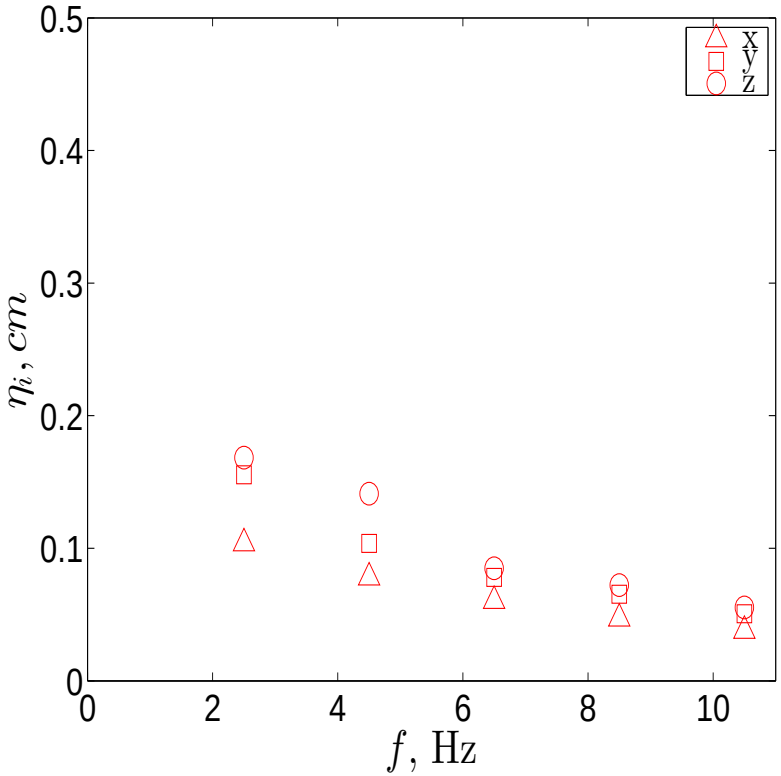

Figure 3.12 : Kolmogorov length components ($\triangle T = 50\,\mathrm{K}$): $\eta = (\nu^3/\varepsilon)^{1/4} \approx \mathrm{Re}^{-3/4}\ell$.

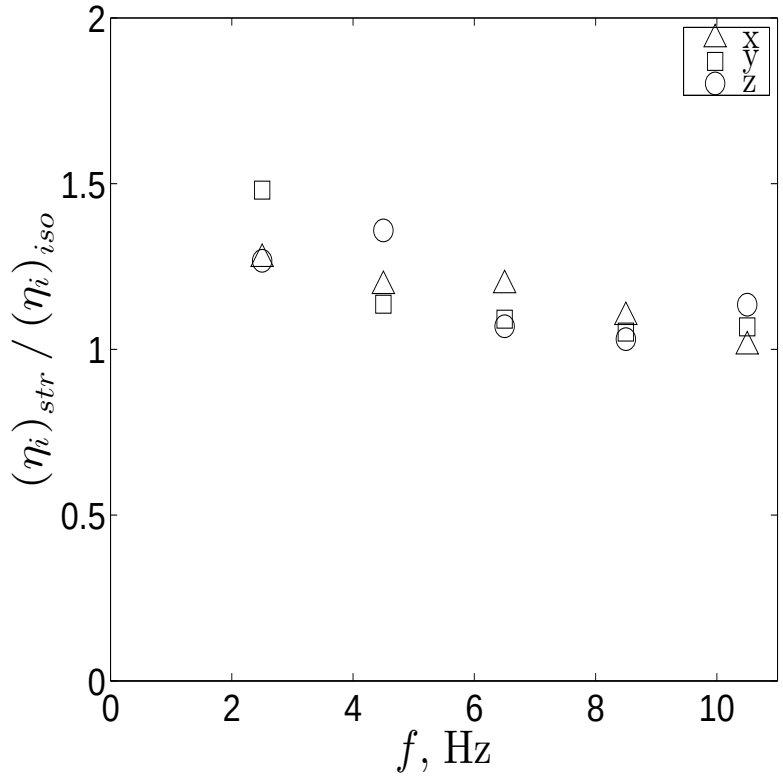

Figure 3.13 : Normalized Kolmogorov scale $(\eta_i)_{str} \,/\, (\eta_i)_{iso}$.

$$\eta_x \approx \eta_y \approx \eta_z$$

Results of PIV measurements

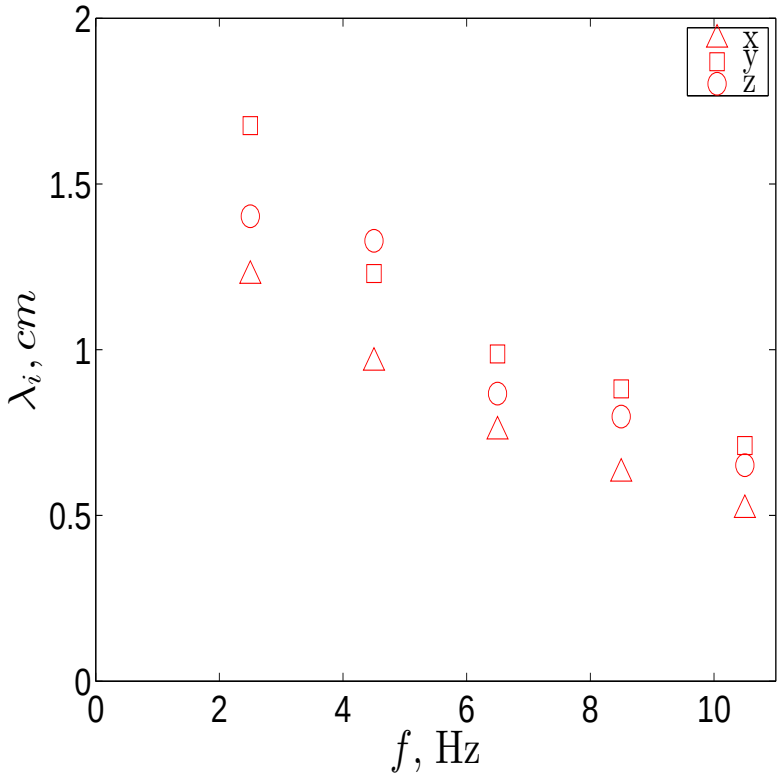

Figure 3.14 : Taylor's microscale components ($\triangle T = 50$ K):
$\lambda = \sqrt{\frac{15\nu}{\varepsilon}}\, u_{rms} \approx \sqrt{15}\mathrm{Re}^{-1/2}\ell$.

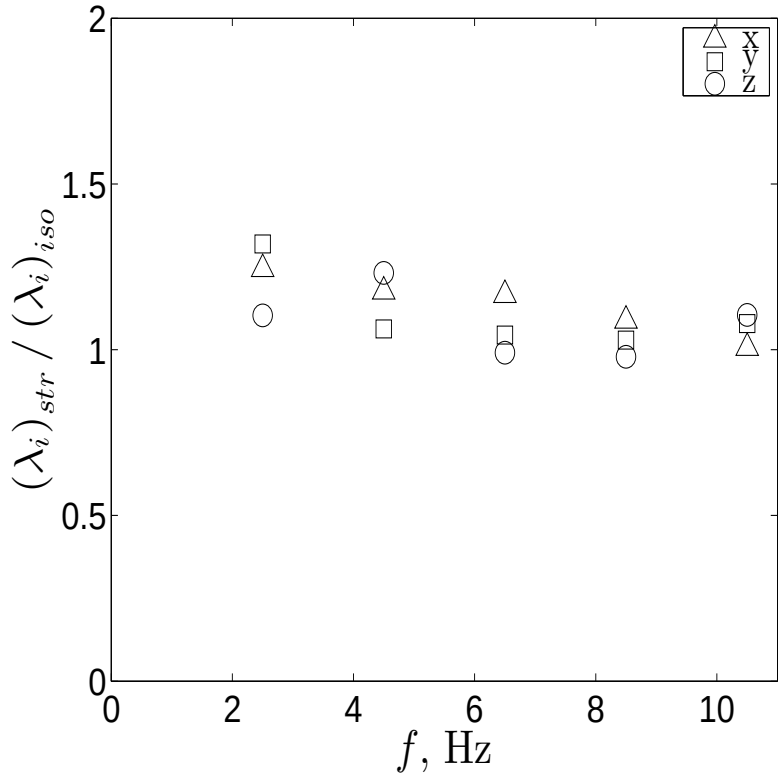

Figure 3.15 : Normalized Taylor scale $(\lambda_i)_{str} \,/\, (\lambda_i)_{iso}$.

Results of PIV measurements

One-dimensional energy density spectra $E_{ii}(k)$,wave length $k = 1/\ell$.

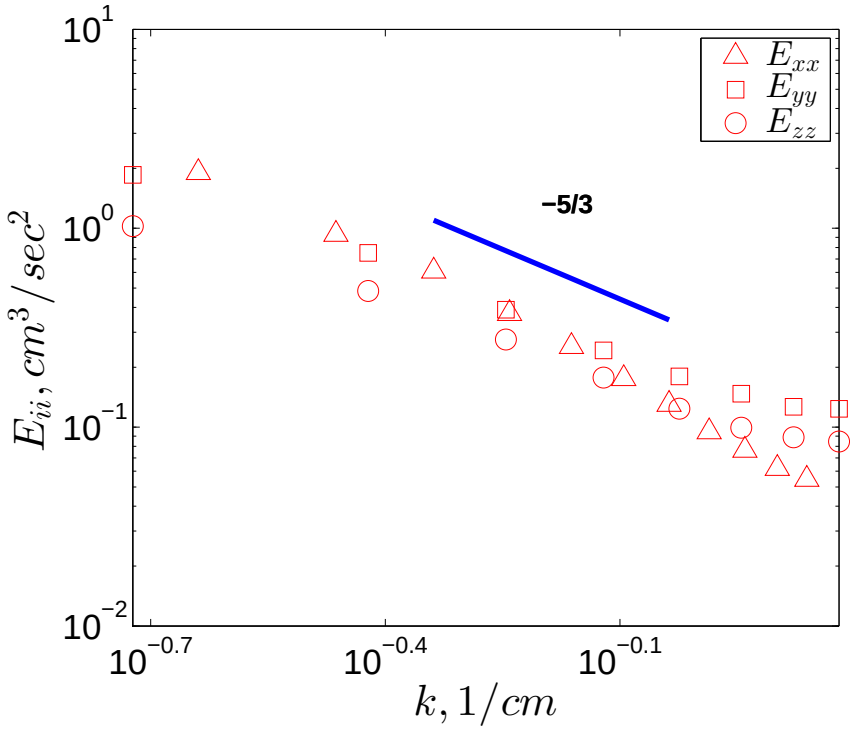

Figure 3.16 : Turbulent energy spectral densities.

Results of temperature measurements

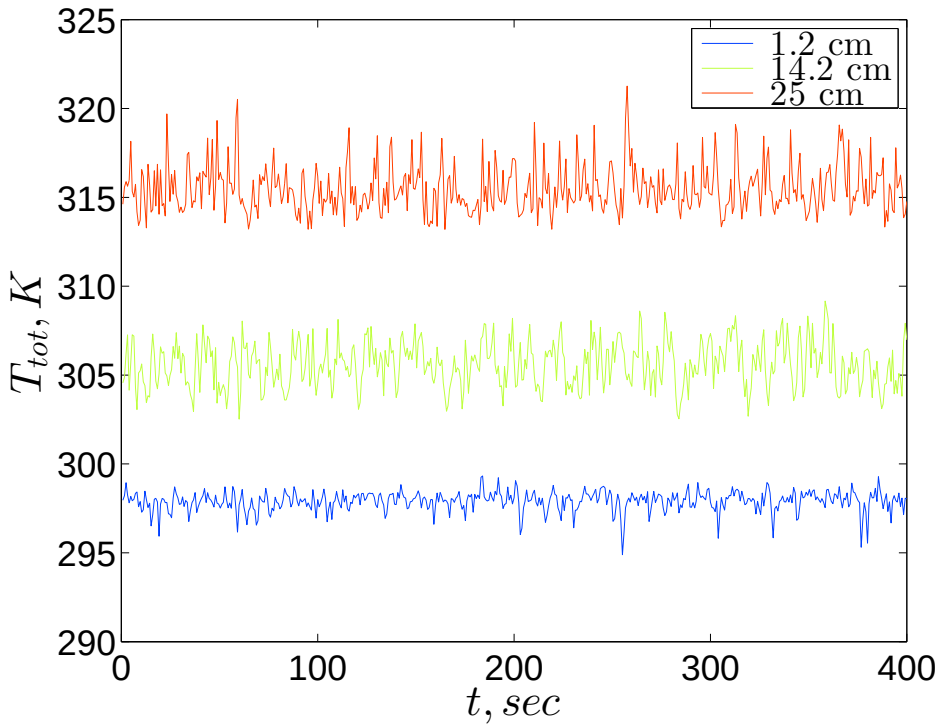

Figure 3.17 : Instantaneous temperature T_{tot} along vertical direction z at the center ($\triangle T = 50$ K,$f = 10.5$ Hz).

Results of temperature measurements

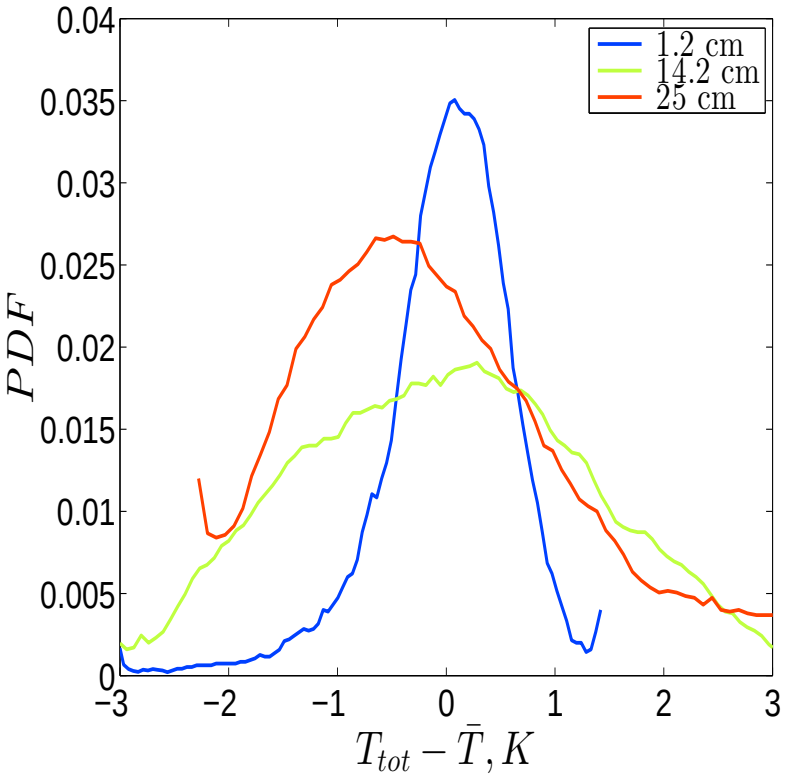

z, cm	1.2	14.2	25.0
$\overline{T}$, K	297.9	305.6	315.6
Θ_{rms}, K	0.56	1.28	1.34
γ_1	-1.3	0.08	1.0
γ_2	6.8	2.4	4.2

Figure 3.18 : PDF of T_{tot} ($\triangle T = 50$ K, $f = 10.5$ Hz).

Expectation value: $\overline{T} = E[T_{tot}]$; standard deviation: $\Theta_{rms} = \sqrt{E\left[\left(T_{tot} - \overline{T}\right)^2\right]}$;

skewness: $\gamma_1 = E\left[\left(T_{tot} - \overline{T}\right)^3\right] / \Theta_{rms}^3$; kurtosis: $\gamma_2 = E\left[\left(T_{tot} - \overline{T}\right)^4\right] / \Theta_{rms}^4$.

Results of temperature measurements

$$T_{tot} = \underbrace{\bar{T} + \delta T}_{T} + \theta = \bar{T} + \underbrace{\delta T + \theta}_{\Theta},$$

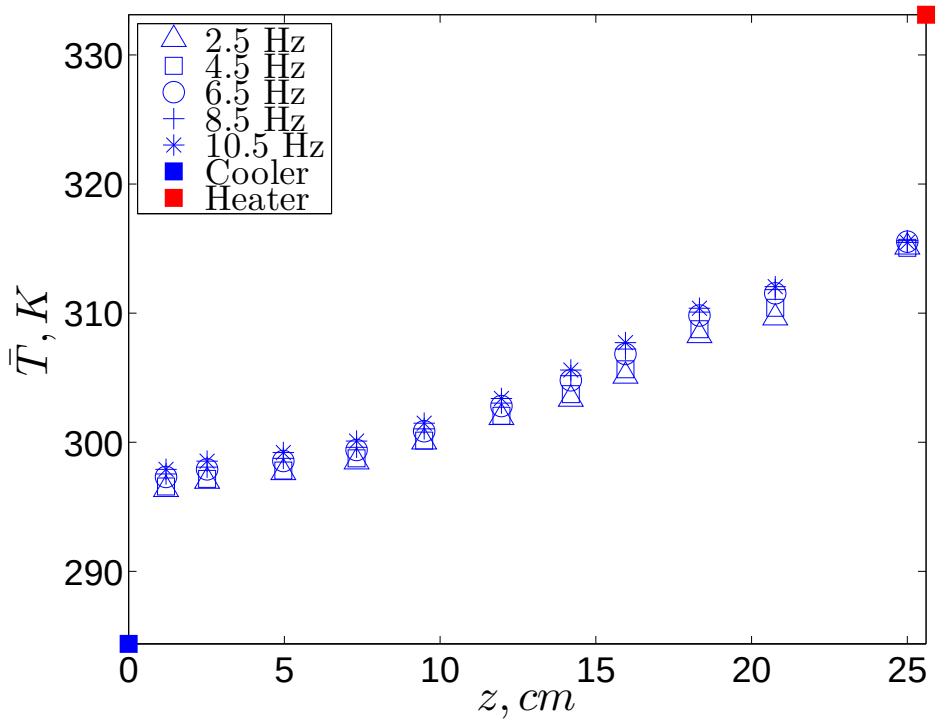

Figure 3.19 : Vertical profile of the mean temperature $\bar{T}(z)$ ($\triangle T = 50$K).

Results of temperature measurements

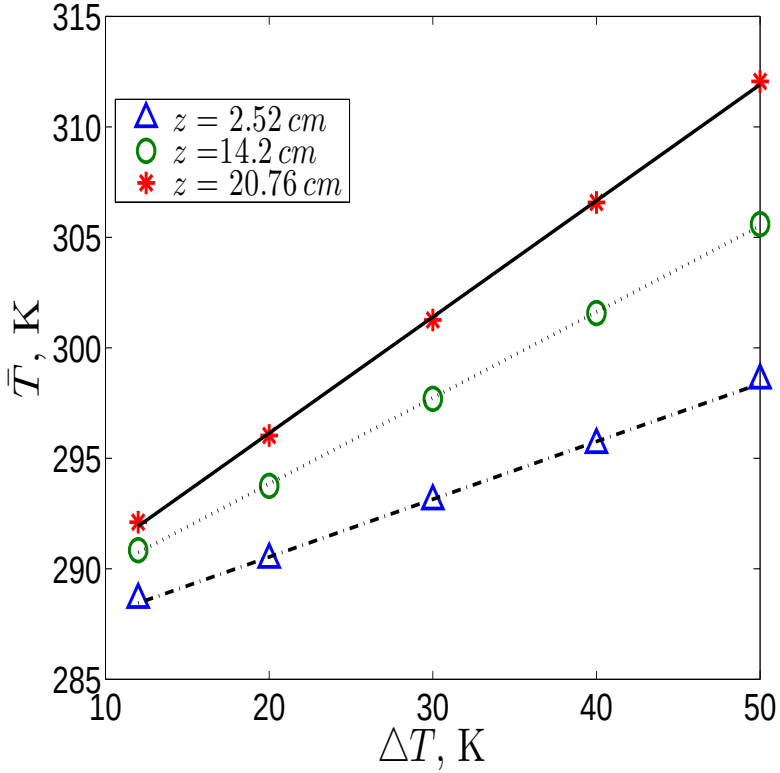

Figure 3.20 : Mean temperature $\bar{T}(z)$ vs. $\triangle T$ ($f = 10.5$ Hz, $\bar{T} = a\triangle T + T_0$), in 3 locations:

$z = 2.5$ cm: $\bar{T} = 0.26\triangle T + 285.3$ K.
$z = 12.2$ cm: $\bar{T} = 0.39\triangle T + 286.0$ K.
$z = 20.8$ cm: $\bar{T} = 0.53\triangle T + 285.6$ K.

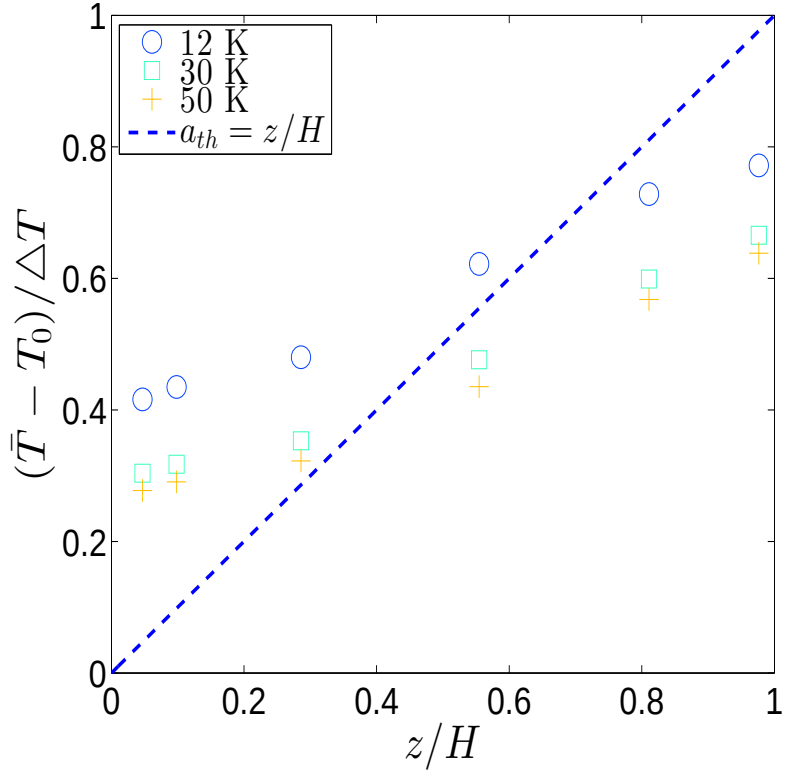

Figure 3.21 : Vertical profile of the mean temperature in dimensionless form ($f = 10.5$ Hz): $(\bar{T}(z) - T_0)/\triangle T$.

Results of temperature measurements

The standard deviation: $\Theta_{rms} = \langle \Theta^2 \rangle^{1/2} = \langle \left(T_{tot} - \overline{T} \right)^2 \rangle^{1/2}$

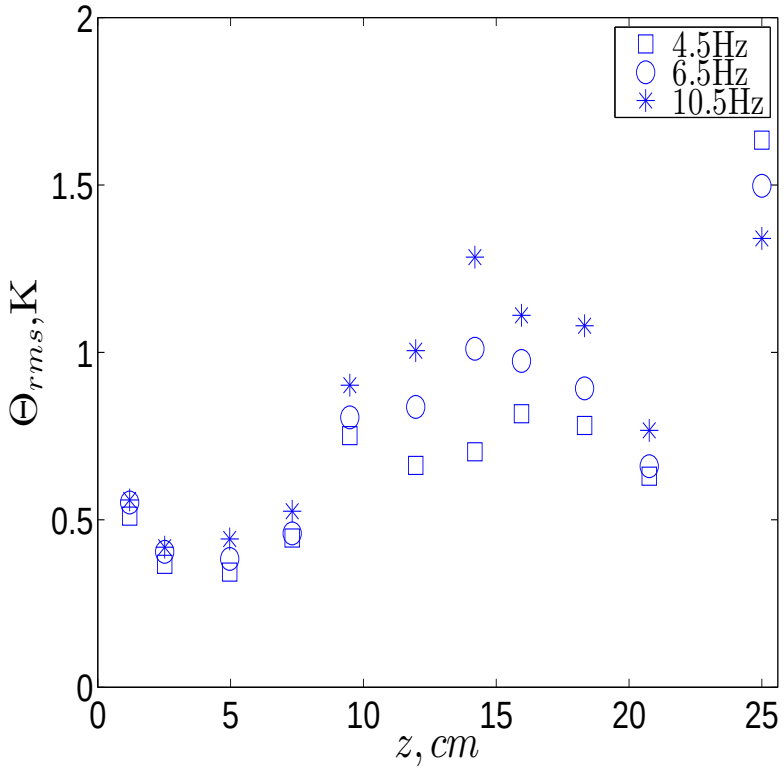

Figure 3.22 : Vertical profile of Θ_{rms}, ($\triangle T = 50$K).

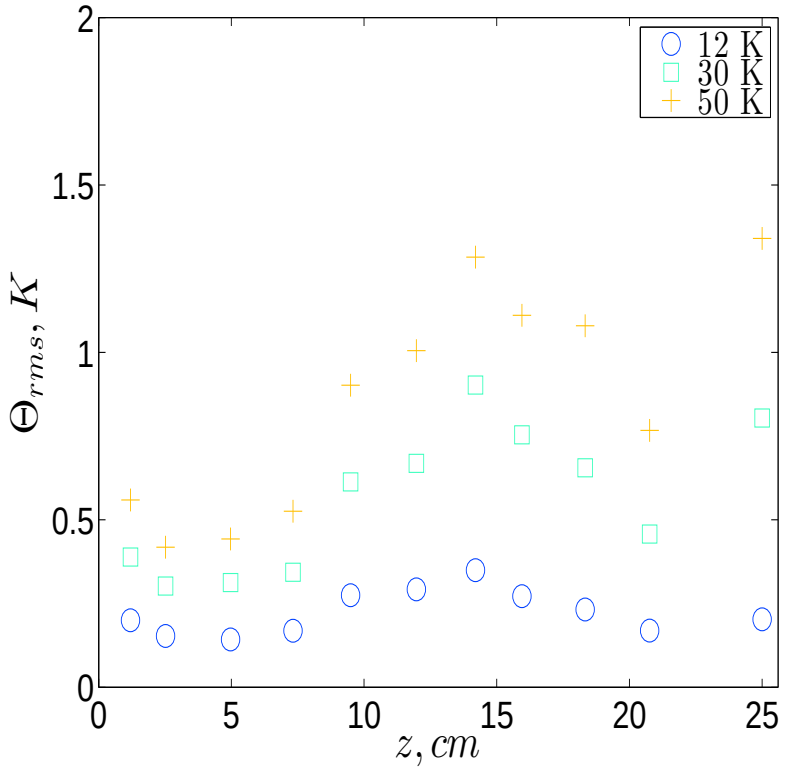

Figure 3.23 : Vertical profile of Θ_{rms} ($f = 10.5$).

Results of temperature measurements

Consider now the central region of the cavity, $10 \times 10 \times 10\, cm^3$.
R.m.s. of the temperature fluctuations, $\theta_{rms} = \sqrt{\langle \theta^2 \rangle}$.

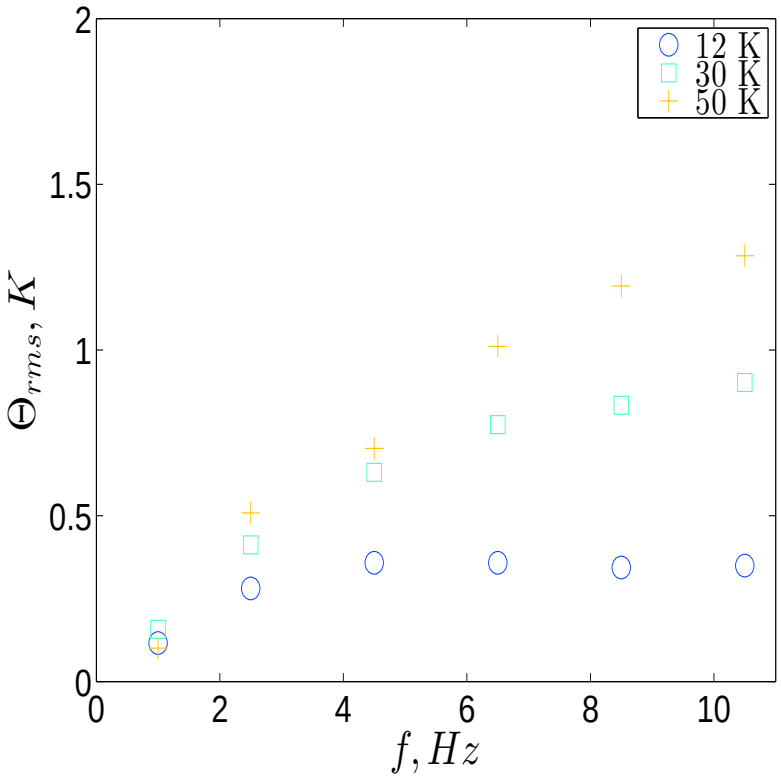

Figure 3.24 :
$\Theta_{rms} = \langle \left(T_{tot} - \overline{T} \right)^2 \rangle^{1/2}$ at the center ($z = 14.2$cm).

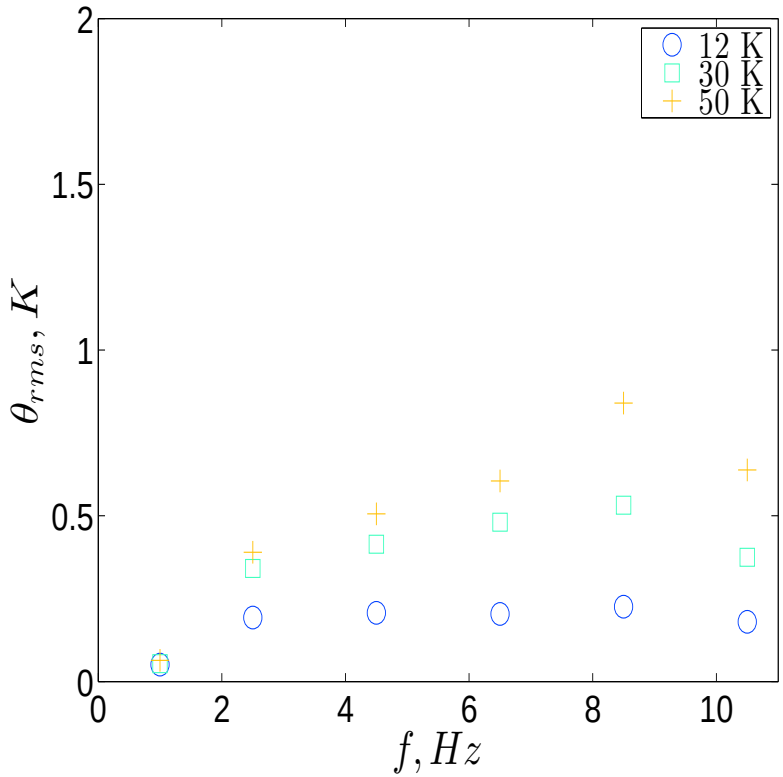

Figure 3.25 : The r.m.s of temperature fluctuations $\theta_{rms} = \sqrt{\langle \theta^2 \rangle}$ at the center ($z = 14.2$cm).

Results of temperature measurements

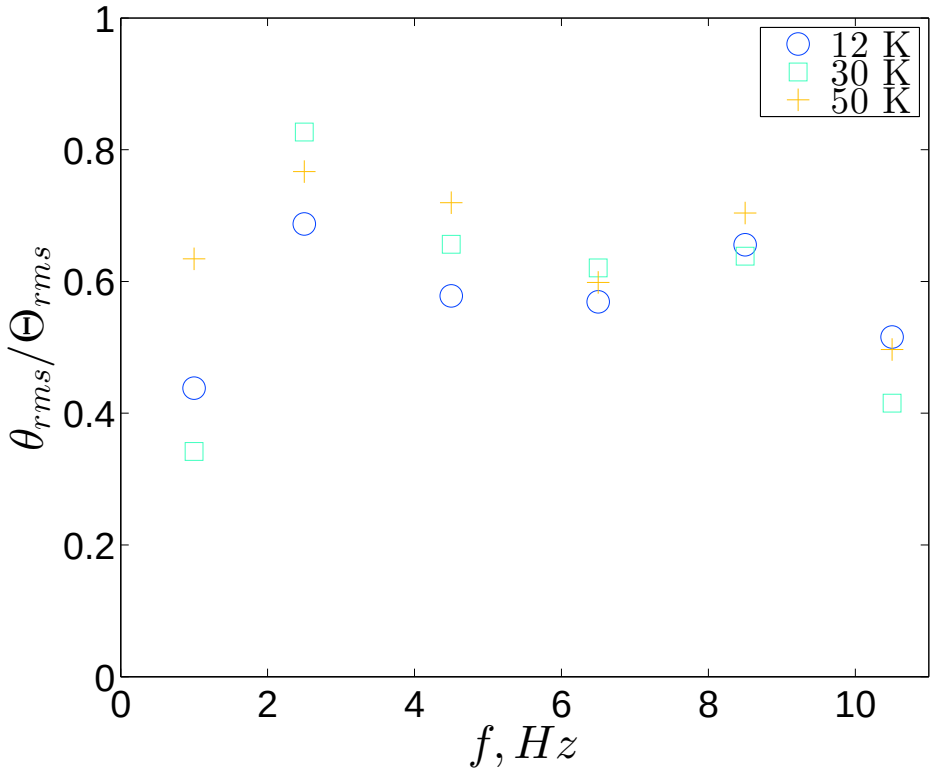

Figure 3.26 : $\theta_{rms}/\Theta_{rms}$.

Contribution of temperature fluctuations θ to temperature oscillations Θ is quite significant.

Results of temperature measurements

$(\delta T)_{\tilde{f}} = \int \delta T \, \exp[-i\tilde{f}\, t]\, dt; \quad E_n(\tilde{f}) = |(\delta T)_{\tilde{f}}|^2 / \int |(\delta T)_{\tilde{f}}|^2 \, d\tilde{f}.$

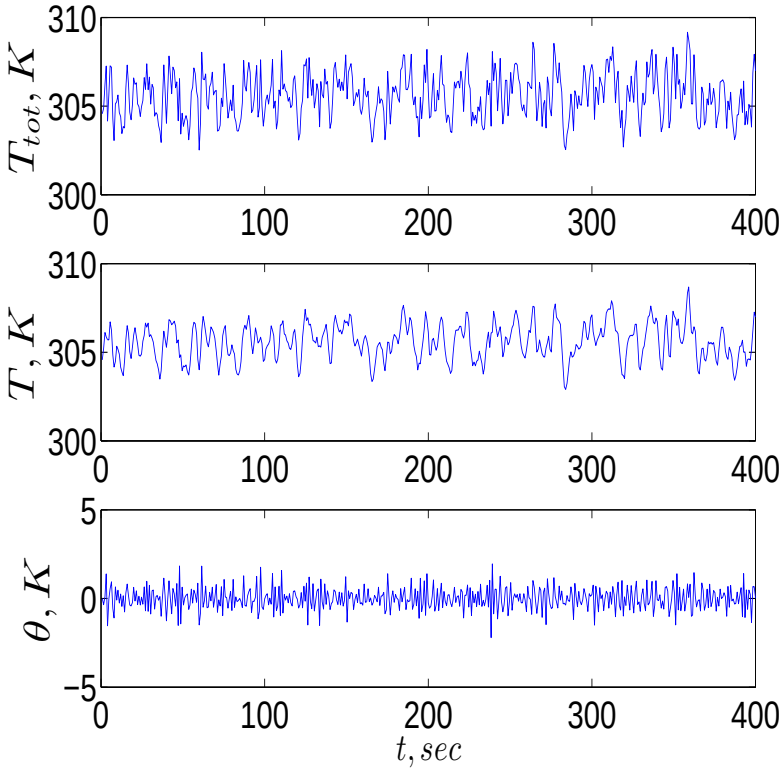

Figure 3.27 : $T_{tot} = T + \theta$ ($z = 14.2\,\text{cm}$, $f = 10.5\,\text{Hz}$, $\triangle T = 50\,\text{K}$).

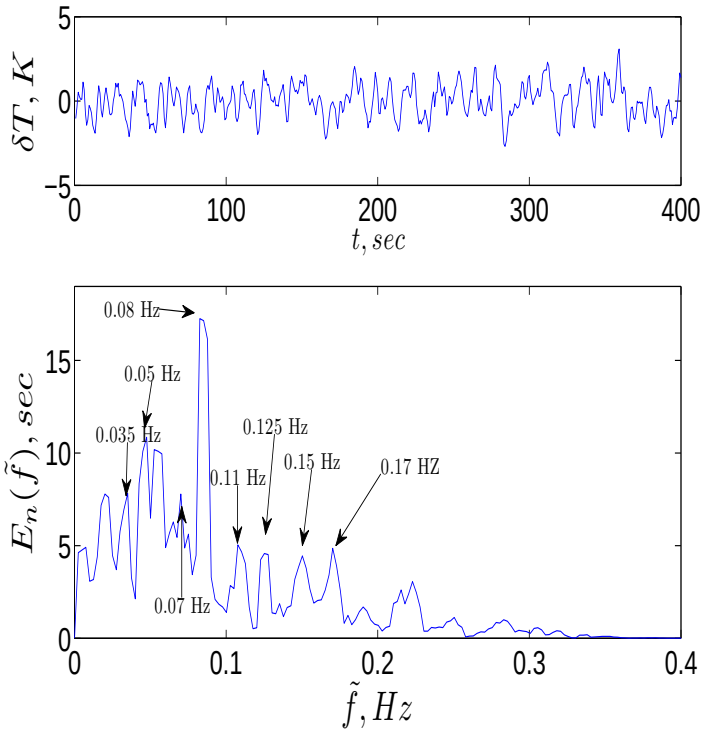

Figure 3.28 : The normalized spectrum function $E_n(\tilde{f})$ of the signal $\delta T = T - \overline{T}$.

Long-term nonlinear variations of δT with the period $\simeq$ 12 s and 20.8 s.

Results of temperature measurements

$$\delta(\nabla_i T) = \nabla_i T - \overline{\nabla_i T}; \quad [\delta(\nabla_i T)]_{rms} = \langle \delta(\nabla_i T)^2 \rangle^{1/2}.$$

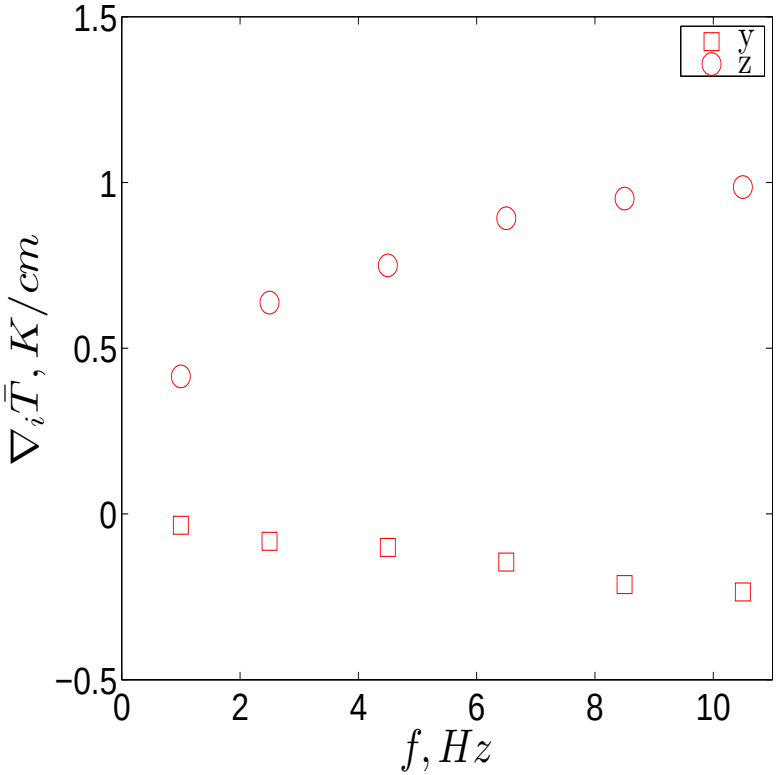

Figure 3.29 : Gradients $\nabla_i \bar{T}$ ($\triangle T = 50\,\mathrm{K}$).

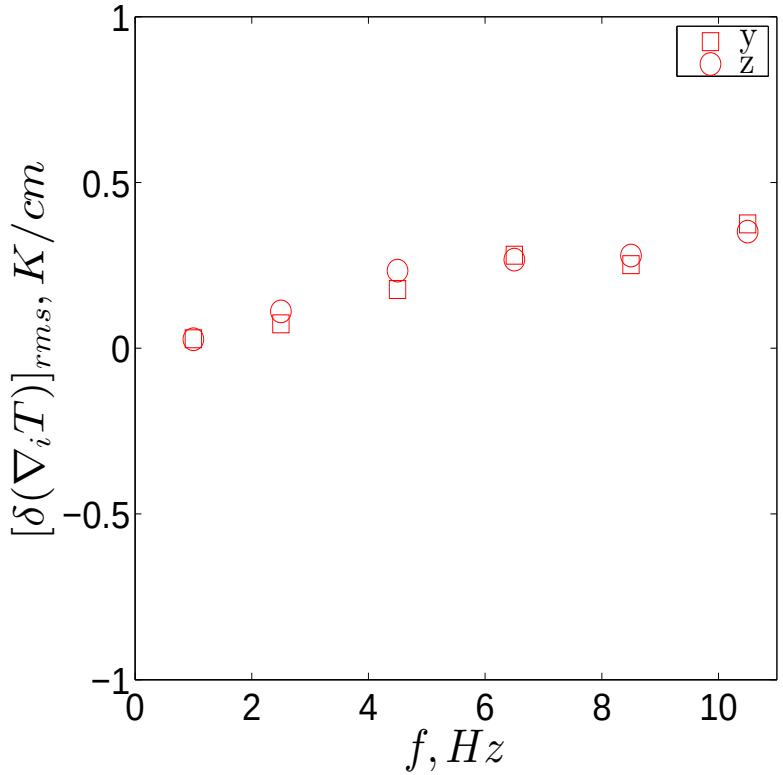

Figure 3.30 : R.m.s of $\delta(\nabla_i T)$ ($\triangle T = 50$ K).

Effect of external forcing on stratified flows characteristics

$N = (\beta \nabla_z \overline{T})^{1/2}, \quad \beta = 1/\overline{T}; \quad Ri_T = N^2 \tau_0^2, \quad \tau_0 = \ell / u_{rms}.$

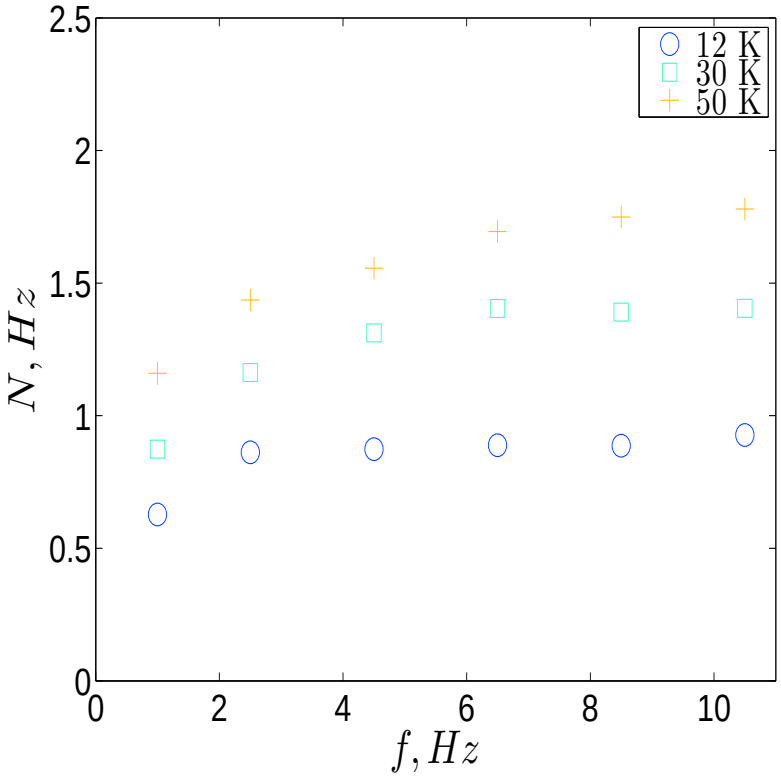

Figure 3.31 : Brunt-Väisälä frequency N.

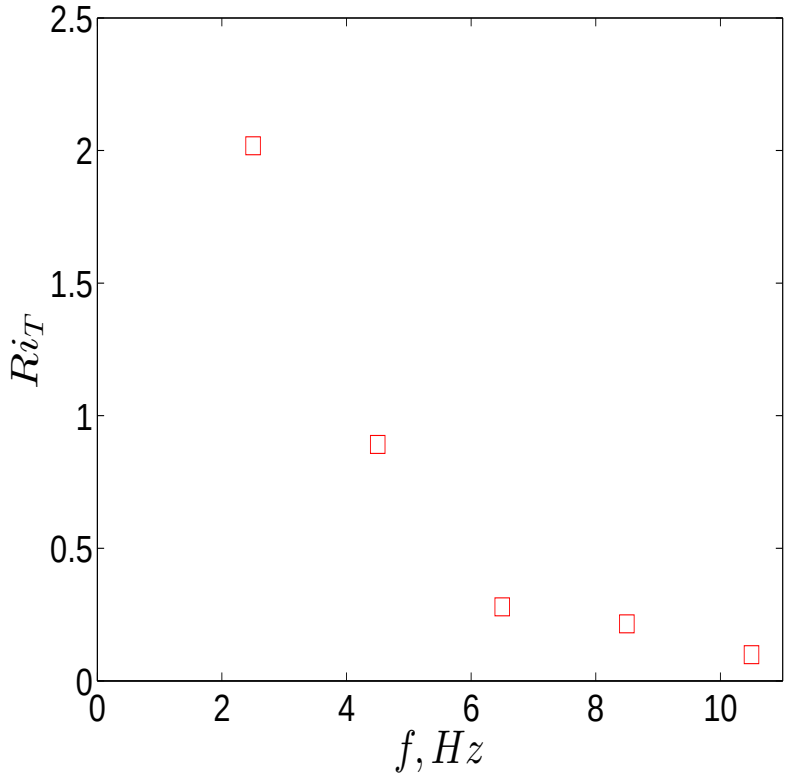

Figure 3.32 : Turbulent Richardson number $Ri_T = N^2 \tau_0^2$ ($\triangle T = 50$ K).

For large frequencies of the grid oscillations whereby $Ri_T \ll 1$, for which the temperature field can be considered as a passive-scalar.

Effect of external forcing on stratified flows characteristics

$[\ell_* \nabla_* T]^2 \equiv [(\ell_x \nabla_x \bar{T})^2 + (\ell_y \nabla_y \bar{T})^2 + (\ell_z \nabla_z \bar{T})^2] \times [1 + 2 C_\theta C_F Ri_T]^{-1}$.

$(u_{rms,z})_{th} = [(u_{z,iso})^2 - C_u \ell_z \beta \sqrt{\langle \theta^2 \rangle}]^{1/2}$.

$\ell_x = \ell_y$.

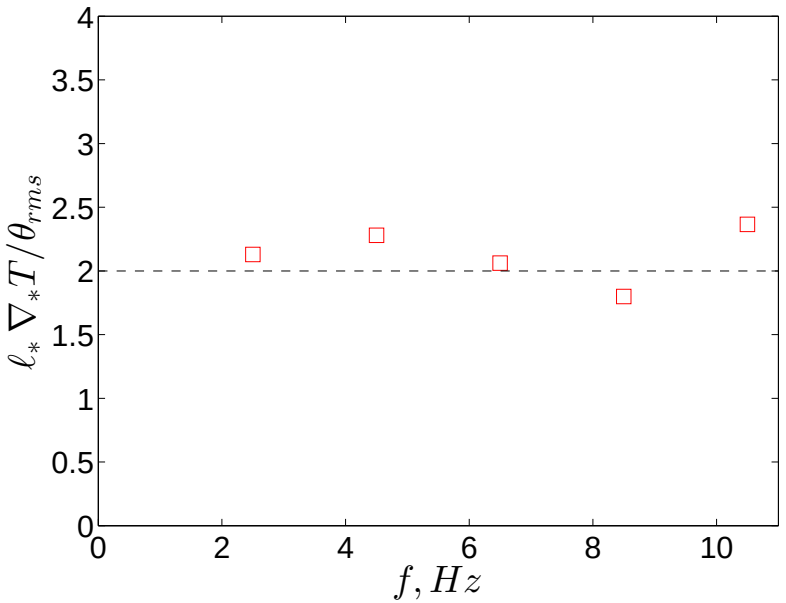

Figure 3.33 : The non-dimensional ratio $\ell_* \nabla_* T / \theta_{rms}$ ($\triangle T = 50\,\mathrm{K}$).

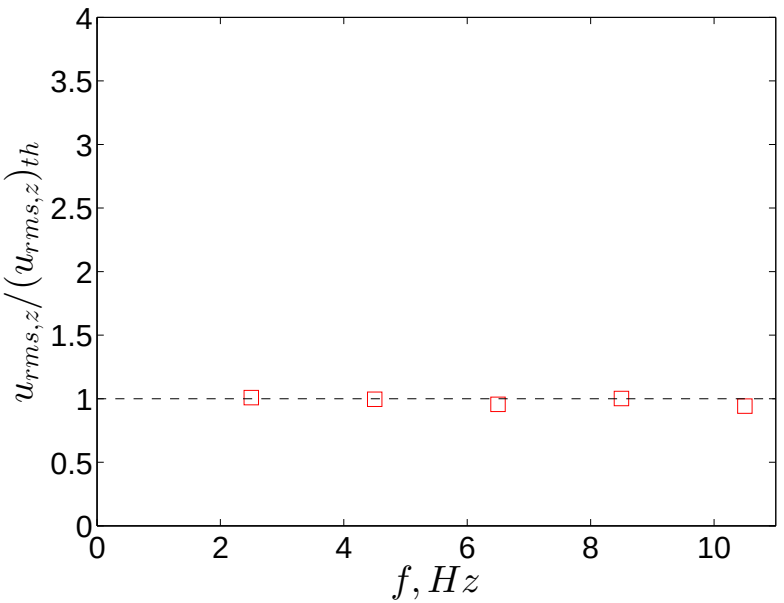

Figure 3.34 : Ratio $u_{rms,z}/(u_{rms,z})_{th}$.

Stably stratified turbulence: $C_F = 0.11$, $C_\theta = 2.7$, $C_u = 1.79$.

Unstably stratified turbulence: $C_F = 0.2$, $C_\theta = 0.83$, $C_u = 4$.

Summary and conclusions

- Distribution of r.m.s velocity components in the central part of the probed region is quite homogeneous and nearly isotropic.
- Larger portion of the turbulent kinetic energy associated with velocity fluctuations in the direction of grid oscillations.
- The central part of the turbulent kinetic energy spectrum has a slope close to $-5/3$. This finding is in compliance with Kolmogorovs -5/3 law for the inertial region.
- Predictions of energy- and flux-budget turbulence closure (EFB) model are in a good agreement with the experimental results.
- Temperature cannot be considered as a passives scalar in most of the range of grid frequencies because Richardson number is small only for large frequencies.
- We detected also long-term nonlinear oscillations of the mean temperature in stably stratified turbulence for all frequencies of grid oscillations similarly to the case of the unstably stratified flows.

Summary and conclusions

The main results obtained in this study were published in the following papers in scientific journals and conference proceedings:

(i) Eidelman, A., Elperin, T., Gluzman, I., Kleeorin, N., and Rogachevskii, I.,Temperature And Velocity Fluctuations In Forced Stably Stratified And Convective Turbulent Flows: Experiments And Theory, 14^{th} *European Turbulence Conference*, Lyon, France, 1-4 September, 2013.

(ii) Eidelman, A., Elperin, T., Gluzman, I., Kleeorin, N., and Rogachevskii, I., Experimental study of temperature fluctuations in forced stably stratified turbulent flows, *Physics of Fluids*, **9**, 201-205, 2012.

(iii) Eidelman, A., Elperin, T., Gluzman, I., Kleeorin, N., and Rogachevskii, I., Experimental study of temperature fluctuations in forced stably stratified turbulent flows, *The 32nd Israeli Conference of Mechanical Engineering*, Tel-Aviv, Israel, October 17-18, 2012.

The End